Brazilian Test
(Diametral Compression of Discs)

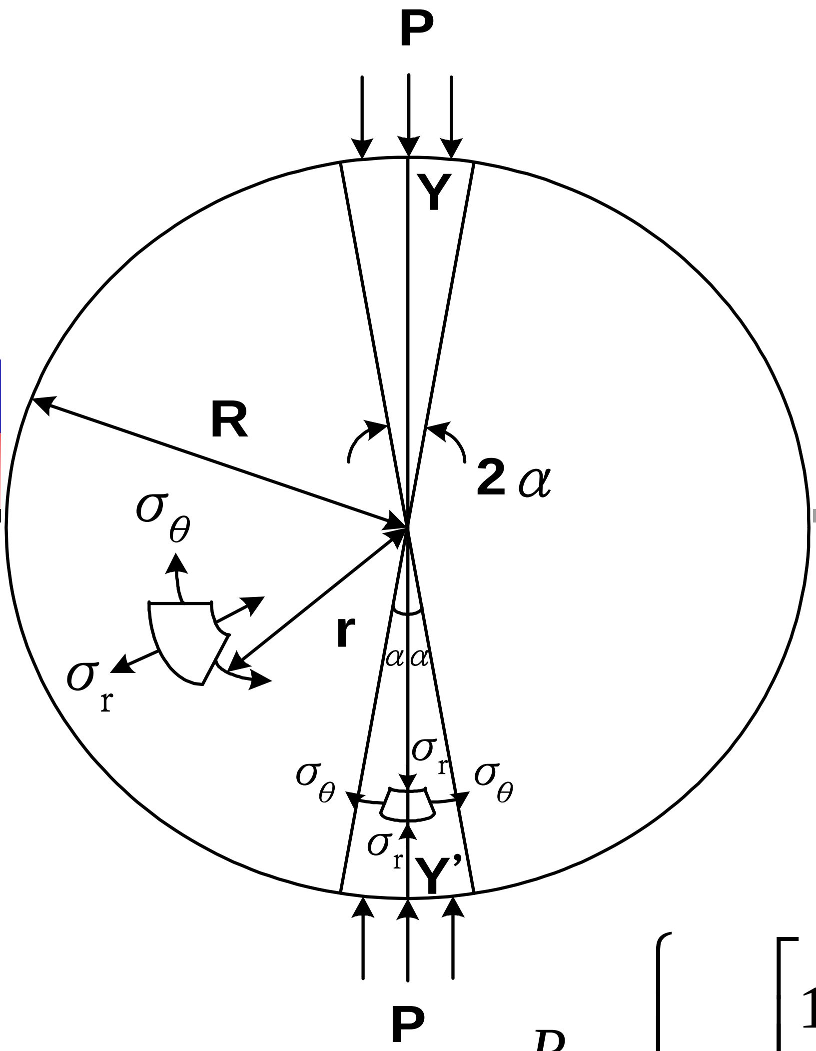

The stress component normal to the loading diameter YY' (σ_θ) (Hondros, 1959)

$$\sigma_\theta = -\frac{P}{\pi R t \alpha}\left\{ \frac{\left[1-(\frac{r}{R})^2\right]\sin 2\alpha}{1-2(\frac{r}{R})^2\cos 2\alpha + (\frac{r}{R})^4} - \tan^{-1}\left[\frac{1+(\frac{r}{R})^2}{1-(\frac{r}{R})^2}\tan\alpha\right]\right\}$$

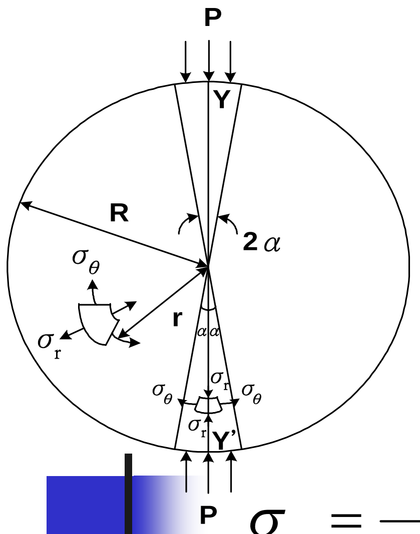

Brazilian Test (Diametral Compression of Discs)

The stress component along YY' (σ_r)

$$\sigma_r = \frac{P}{\pi R t \alpha}\left\{ \frac{\left[1-(\frac{r}{R})^2\right]\sin 2\alpha}{1-2(\frac{r}{R})^2\cos 2\alpha + (\frac{r}{R})^4} + \tan^{-1}\left[\frac{1+(\frac{r}{R})^2}{1-(\frac{r}{R})^2}\tan\alpha\right]\right\}$$

where σ_θ : **stress component normal to the loading diameter**

σ_r : **stress component along the loading diameter**

P : **applied force**

r : **distance from the center of disc**

t : **thickness of the disc**

2α : **angular distance over which P is assumed to be distributed radially**

R : **radius of the disc**

Brazilian Test (Diametral Compression of Discs)

σ_θ 及 σ_r差別在 $\tan^{-1}$ 前的加減號及最前面的正、負號

$$\sigma_\theta = -\frac{P}{\pi R t \alpha}\left\{\frac{\left[1-(\frac{r}{R})^2\right]\sin 2\alpha}{1-2(\frac{r}{R})^2\cos 2\alpha+(\frac{r}{R})^4} - \tan^{-1}\left[\frac{1+(\frac{r}{R})^2}{1-(\frac{r}{R})^2}\tan\alpha\right]\right\}$$

$$\sigma_r = \frac{P}{\pi R t \alpha}\left\{\frac{\left[1-(\frac{r}{R})^2\right]\sin 2\alpha}{1-2(\frac{r}{R})^2\cos 2\alpha+(\frac{r}{R})^4} + \tan^{-1}\left[\frac{1+(\frac{r}{R})^2}{1-(\frac{r}{R})^2}\tan\alpha\right]\right\}$$

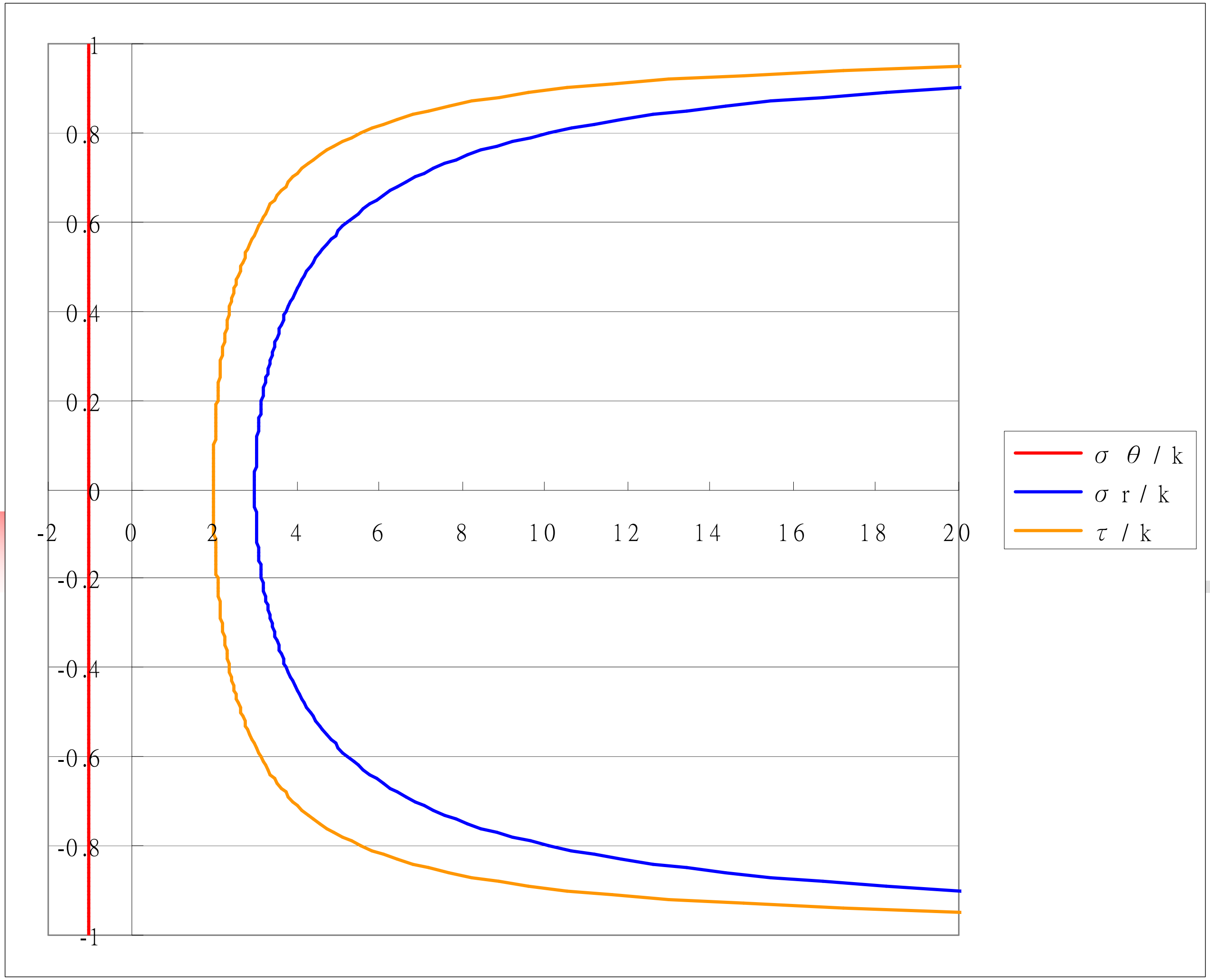

$$k = \frac{P}{\pi R t}$$

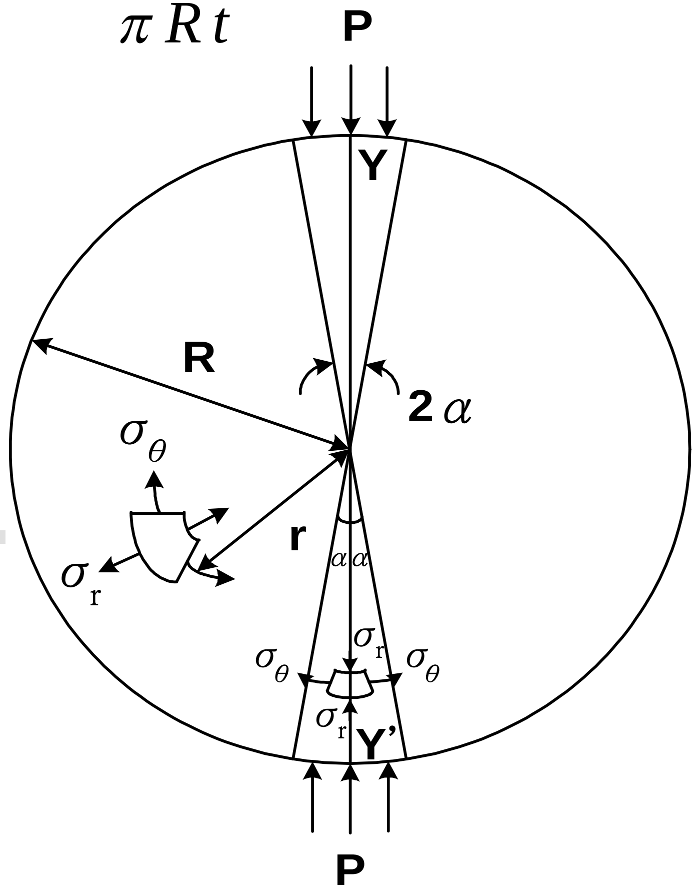

$$\sigma_\theta = -\frac{P}{\pi R t \alpha}\left\{\frac{\left[1-(\frac{r}{R})^2\right]\sin 2\alpha}{1-2(\frac{r}{R})^2\cos 2\alpha+(\frac{r}{R})^4}-\tan^{-1}\left[\frac{1+(\frac{r}{R})^2}{1-(\frac{r}{R})^2}\tan\alpha\right]\right\}$$

$$\sigma_r = \frac{P}{\pi R t \alpha}\left\{\frac{\left[1-(\frac{r}{R})^2\right]\sin 2\alpha}{1-2(\frac{r}{R})^2\cos 2\alpha+(\frac{r}{R})^4}+\tan^{-1}\left[\frac{1+(\frac{r}{R})^2}{1-(\frac{r}{R})^2}\tan\alpha\right]\right\}$$

Brazilian Test (Diametral Compression of Discs)

當試體承受線荷重(即 α 很小)，則在圓心處($r=0$)張力最大

If $r=0$

$$\sigma_\theta = -\frac{P}{\pi R t}\left[\frac{\sin 2\alpha}{\alpha} - 1\right] \approx -\frac{P}{\pi R t} = \sigma_t = -\frac{2P}{\pi D t} = \frac{0.636P}{Dt}$$

$$\sigma_r = \frac{P}{\pi R t}\left[\frac{\sin 2\alpha}{\alpha} + 1\right] \approx \frac{3P}{\pi R t} = \frac{6P}{\pi D t} = -3\sigma_t$$

在圓心處壓力為張力的**3**倍，但 σ_c/σ_t一般在**8～50**，故將產生張力破壞

Brazilian Test (Diametral Compression of Discs)

- Bazilian test has been found to give tensile strength higher than that of direct tension test, probably owing to the effect of fissures. Short fissures weaken a direct tension specimen more severely than they weaken a splitting tension specimen. The ratio has been found to vary from 1 to more than ten as length of preexisting fissures grows larger.

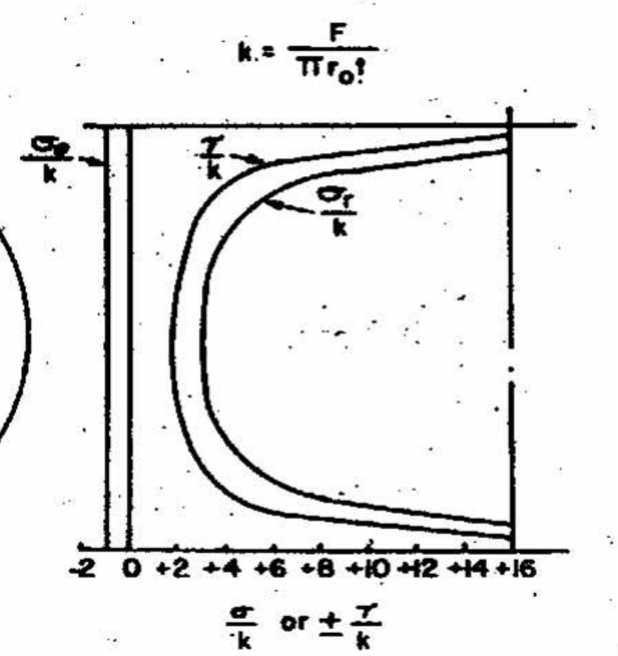

F
A
B
F
k = F / π r₀ t
σθ / k
τ / k
σr / k
-2 0 +2 +4 +6 +8 +10 +12 +14 +16
σ / k or ± τ / k

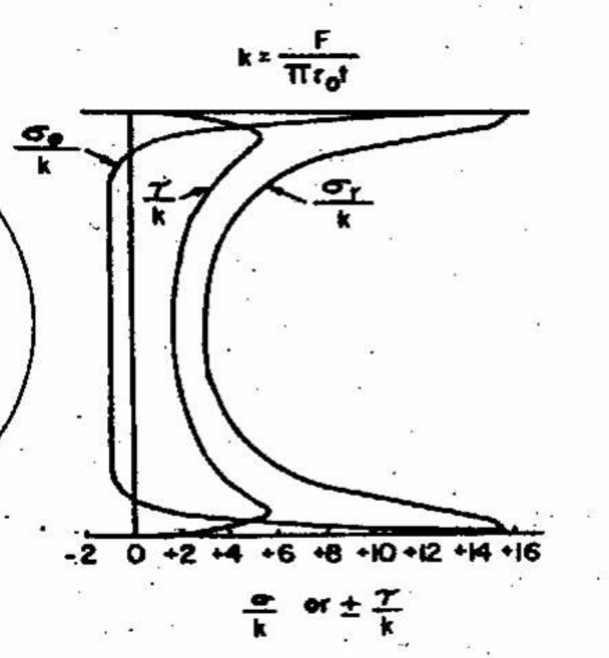

F
A
B
F
k = F / π r₀ t
σθ / k
τ / k
σr / k
-2 0 +2 +4 +6 +8 +10 +12 +14 +16
σ / k or ± τ / k

Brazilian Test (Diametral Compression of Discs)

1.試簡述下列各試驗之方法與目的：**(88**檢覈**)**

(一**)**岩石巴西人法試驗**(Brazilian test)**

(註：必要時，請輔以簡圖說明之**)**

2.請列舉數種岩石試體張力強度之試驗方法，並比較各種方法之優劣。**(15**分**)(8**專技**)(85**應地**)**

3.在實驗室內，求取岩石材料張力強度的方法有那些？請說明其求法？**(15**分**)**

Brazilian Test (Diametral Compression of Discs)

1.若有一圓板，直徑為ｄ，厚**l**，在圓板上下端施加集中荷重Ｐ，則圓板內部任意點Ａ處所受應力為：

$$\sigma_x = \frac{2P}{\pi \ell}\left(\frac{\sin^2\theta_1 \cos\theta_1}{r_1} + \frac{\sin^2\theta_2 \cos\theta_2}{r_2}\right) - \frac{2P}{\pi d \ell}$$

$$\sigma_y = \frac{2P}{\pi \ell}\left(\frac{\cos^3\theta_1}{r_1} + \frac{\cos^3\theta_2}{r_2}\right) - \frac{2P}{\pi d \ell}$$

$$\tau_{xy} = \frac{2P}{\pi \ell}\left(\frac{\cos^2\theta_1 \sin\theta_1}{r_1} + \frac{\cos^2\theta_2 \sin\theta_2}{r_2}\right)$$

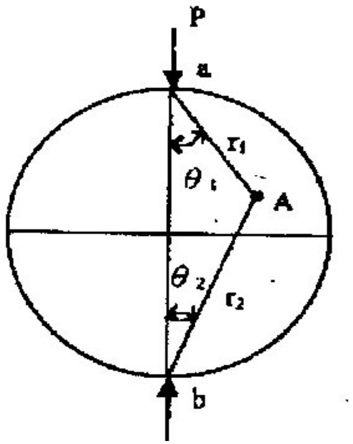

依此原理，製作圓板形岩石試體，進行壓製試驗，又稱巴西試驗（Ｂ**razilianTest**），請繪出**a**，**b**間之σ_x，σ_y，τ_{xy}的變化，並說明應如何求試體的張力強度。**(20**分**)**

Brazilian Test (Diametral Compression of Discs)

1.解釋或說明下列各項：**(91**專技**)**

說明完整岩心在進行巴西抗張試驗時，圓盤試體中心位置之應力狀態。**(5**分**)**

1.有數公尺甚爲完整，不具不連續面，且具有相同岩性之岩心，其直徑爲**50mm**，平均岩石密度爲**0.025MN/m³**，經以下一系列之試驗：

(一**)**徑向點荷重試驗，得平均破壞荷重爲**5KN(Kilo-Newton)**

(二**)**單壓試驗，得平均破壞荷重爲**100KN**

(三**)**巴西試驗，得平均破壞荷重爲**10KN(**厚度爲直徑一半**)**

(四**)**超音波試驗，得平均縱波波速爲**3500m/sec**，平均橫波波速爲**2000m/sec**

請回答：

(一**)**本岩石之張力強度爲何？**(5**分**)**

(二**)**本岩石動態彈性係數爲何？**(10**分**)**

(三**)**未來類似之岩石如何由徑向點荷重試驗結果估計其單壓強度？**(5**分**)**

Brazilian Test (Diametral Compression of Discs)

1.以直徑**5**公分之乾燥岩心進行試驗，得結果如下：

(一**)**巴西劈裂試驗：岩心直徑**5**公分，厚度**3**公分，劈裂荷重 **= 236 kgf**

(二**)**一軸壓縮試驗：岩心直徑**5**公分，高度**10**公分，壓縮破壞荷重 **= 1570kgf**

(三**)**三軸壓縮試驗：岩心直徑**5**公分，高度**10**公分，試驗結果：

圍 壓(kgf/cm^2)	破壞時之軸差荷重 (kgf)
20	2160
40	2900
80	3965

請將此三種試驗的破壞莫爾（**Mohr**）應力圓繪出，並繪製莫爾－庫倫破壞準則**(Mohr**－**Coulomb criterion)**，以及預測圍壓爲**70** kgf/cm^2時，岩心試體破壞強度和破壞面之角度。**(25**分**)**

Brazilian Test (Diametral Compression of Discs)

Read

(1).Vutukuri, Lama and Saluja, vol.1, p.15~111 (1974).

(2).Jaeger and Cook, "Fundamental of Rock Mechanics" p.169~170 and p.258~260 (1979).

(3).Brown, "ISRM Suggested Methods", p.120~121 (1981).

(4).ASTM D3967-86 "Standard Method for Spliting Tensile Strength of Intact Rock Core Specimens".

4.4 Behaviour of isotropic rock material in multiaxial compression

4.4. I Types of multiaxial compression test

Biaxial compression ($\sigma_1 \geq \sigma_2 , \sigma_3 = 0$)

Triaxial compression ($\sigma_1 > \sigma_2 = \sigma_3$) Conventional Triaxial

Polyaxial compression ($\sigma_1 > \sigma_2 > \sigma_3$)

True Triaxial

4.4.2 Biaxial compression ($\sigma_1 \geq \sigma_2$, $\sigma_3 = 0$)

Biaxial compression tests are carried out by applying different normal stresses to two pairs of faces of a cube, plate or rectangular prism of rock.

4.4.2 Biaxial compression ($\sigma_1 \geq \sigma_2$, $\sigma_3 = 0$)

The great difficulty with such tests is that the end effects described in section 4.3.3 exert an even greater influence on the stress distribution within the specimen than in the case of uniaxial compression. For

this reason, fluid rather than solid medium loading is preferred.

4.4.2 Biaxial compression ($\sigma_1 \geq \sigma_2 , \sigma_3 = 0$)

Brown (1974) carried out a series of biaxial compression tests on 76 mm square by 25 mm thick plates of Wombeyan Marble which were loaded on their smaller faces through (a) 76 mm x 25 mm solid steel platens, and (b) brush platens made from 3.2 mm square steel pins.

4.4.2 Biaxial compression ($\sigma_1 \geq \sigma_2, \sigma_3 = 0$)

Figure 4.15 shows the peak strength envelopes obtained in tests carried out at constant ratios. The data are normalised with respect to the uniaxial compressive strength of the plates σ_c = 66 MPa.

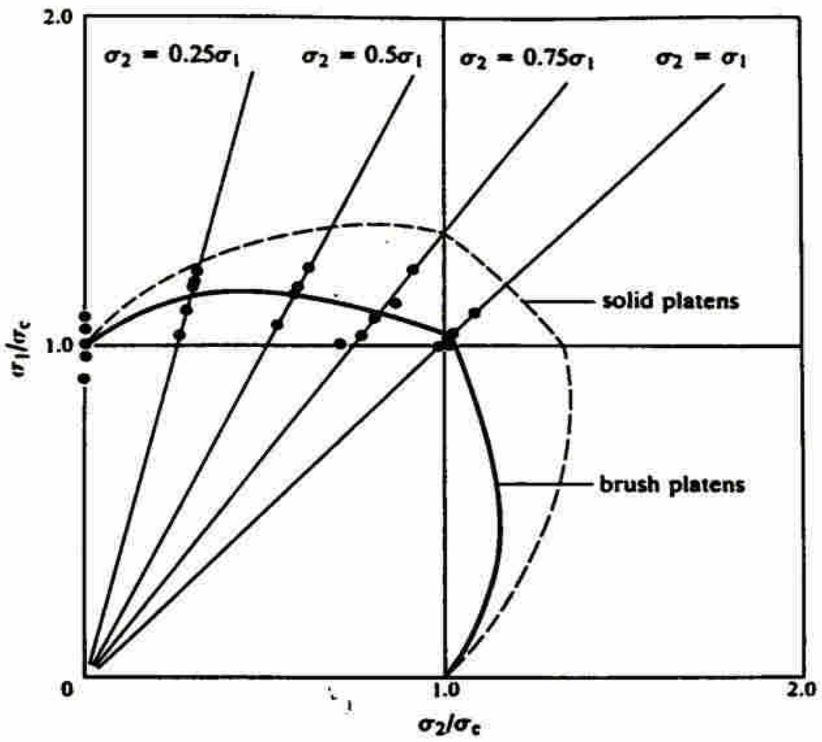

Figure 4.15 Biaxial compression test results for Wombeyan Marble (after Brown, 1974).

4.4.2 Biaxial compression ($\sigma_1 \geq \sigma_2, \sigma_3 = 0$)

This was attributed to the influence of end effects. When the brush platens were used, the maximum measured increase in peak strength over σ_c was only 15%. For $\sigma_2 = \sigma_1$, no strength increase. The practical consequence of these results is that, for this rock type, the 'strengthening' effect of the intermediate principal stress can be neglected so that the uniaxial compressive strength, σ_c , should be used as the rock material strength whenever $\sigma_3 = 0$. This slightly conservative conclusion is likely to apply to a wide range of rock types.

4.4.3 Triaxial compression ($\sigma_1 > \sigma_2 = \sigma_3$)

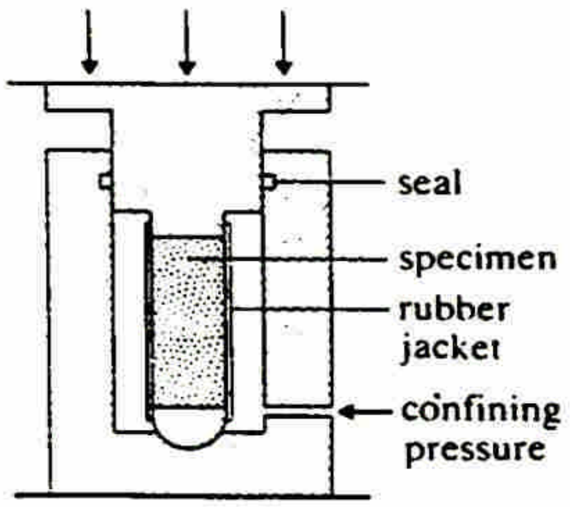

Figure 4.16 Elements of a conventional triaxial testing apparatus.

The specimen is placed inside a pressure vessel (Figures 4.16 and 4.17) and a fluid pressure, σ_3, is applied to its surface. A jacket, usually made of a rubber compound, is used to isolate the specimen from the confining fluid which is usually oil. The axial stress, σ_1, is applied to the specimen via a ram passing through a bush in the top of the cell and hardened steel end caps.

4.4.3 Triaxial compression ($\sigma_1 > \sigma_2 = \sigma_3$)

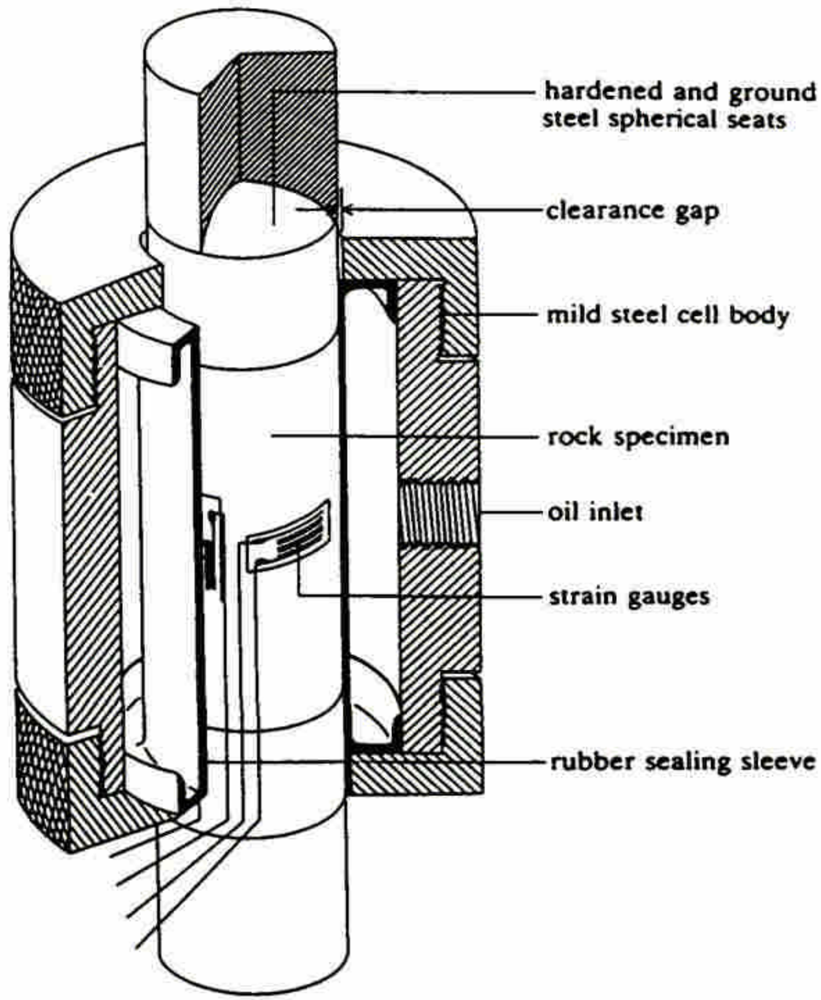

Figure 4.17 Cut-away view of the triaxial cell designed by Hoek and Franklin (1968). Because this cell does not require drainage between tests, it is well suited to carrying out large numbers of tests quickly.

4.4.3 Triaxial compression ($\sigma_1 > \sigma_2 = \sigma_3$)

Axial deformation of the specimen may be most conveniently monitored by linear variable differential transformers (LVDTs) mounted inside or outside the cell, but preferably inside. Local axial and circumferential strains may be measured by electric resistance strain gauges attached to the surface of the specimen (Figure 4.17).

4.4.3 Triaxial compression ($\sigma_1 > \sigma_2 = \sigma_3$)

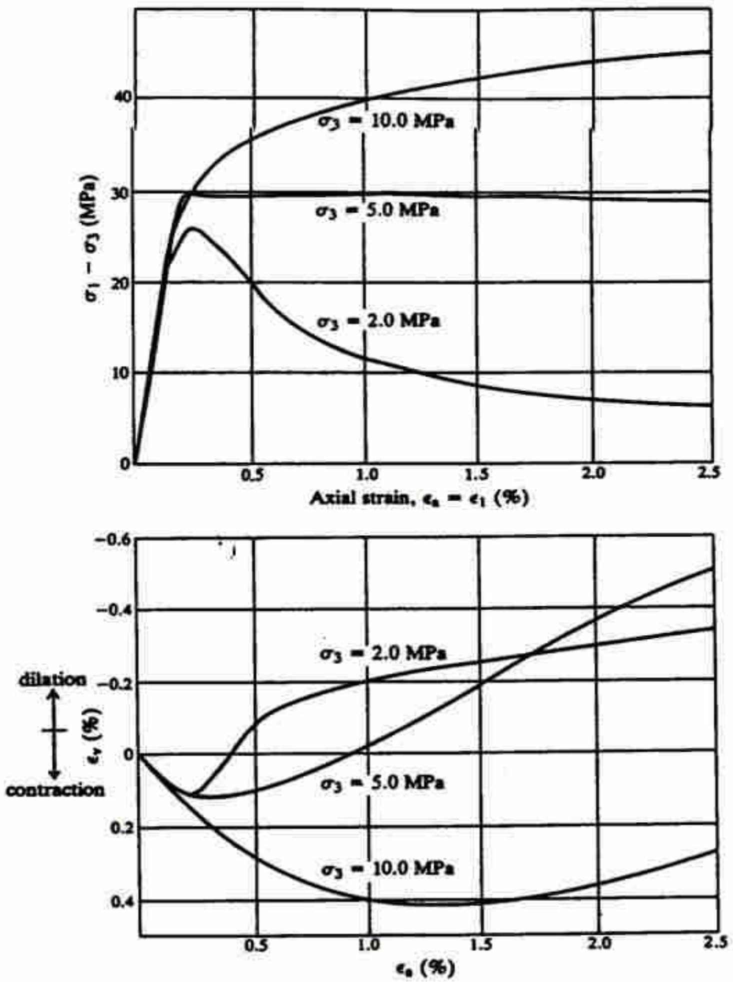

Figure 4.18 Results of triaxial compression tests on an oolitic limestone with volumetric strain measurement (after Elliott, 1982).

Figure 4.18 shows some results obtained using such a system in tests carried out at three different confining pressures on specimens of an oolitic limestone. An important feature of the behaviour of rock material in triaxial compression is illustrated by Fig4.18.

4.4.3 Triaxial compression ($\sigma_1 > \sigma_2 = \sigma_3$)

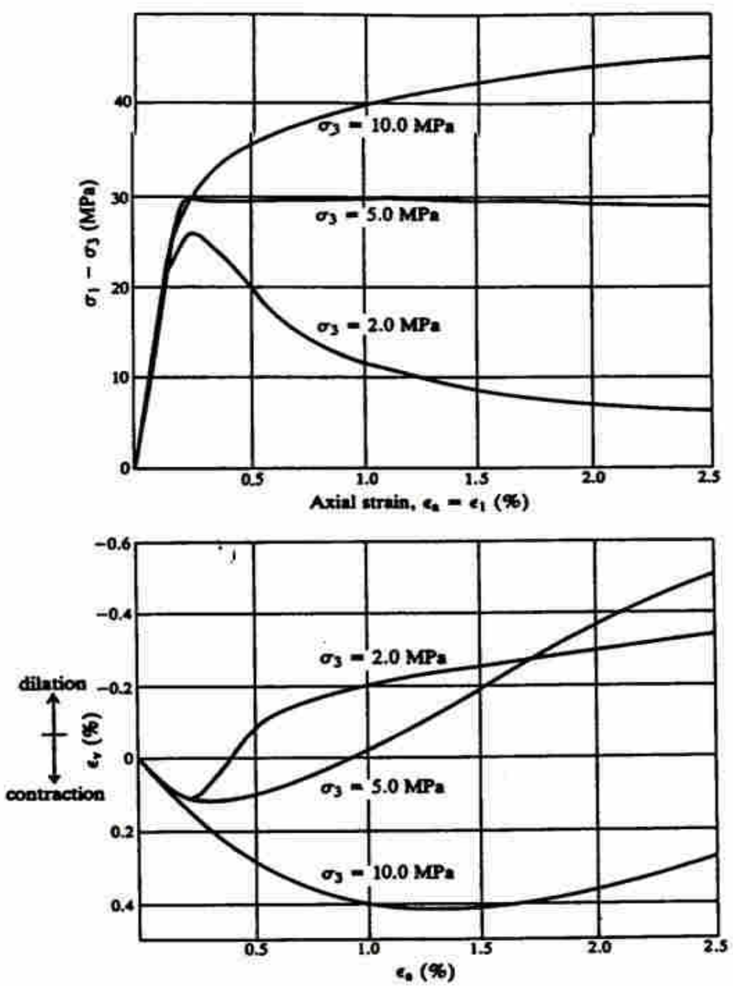

Figure 4.18 Results of triaxial compression tests on an oolitic limestone with volumetric strain measurement (after Elliott, 1982).

When the specimen is initially loaded it compresses, but a point is soon reached, generally before the peak of the axial stress-axial strain curve, at which the specimen begins to dilate (increase in volume) as a result of internal fracturing.

4.4.3 Triaxial compression ($\sigma_1 > \sigma_2 = \sigma_3$)

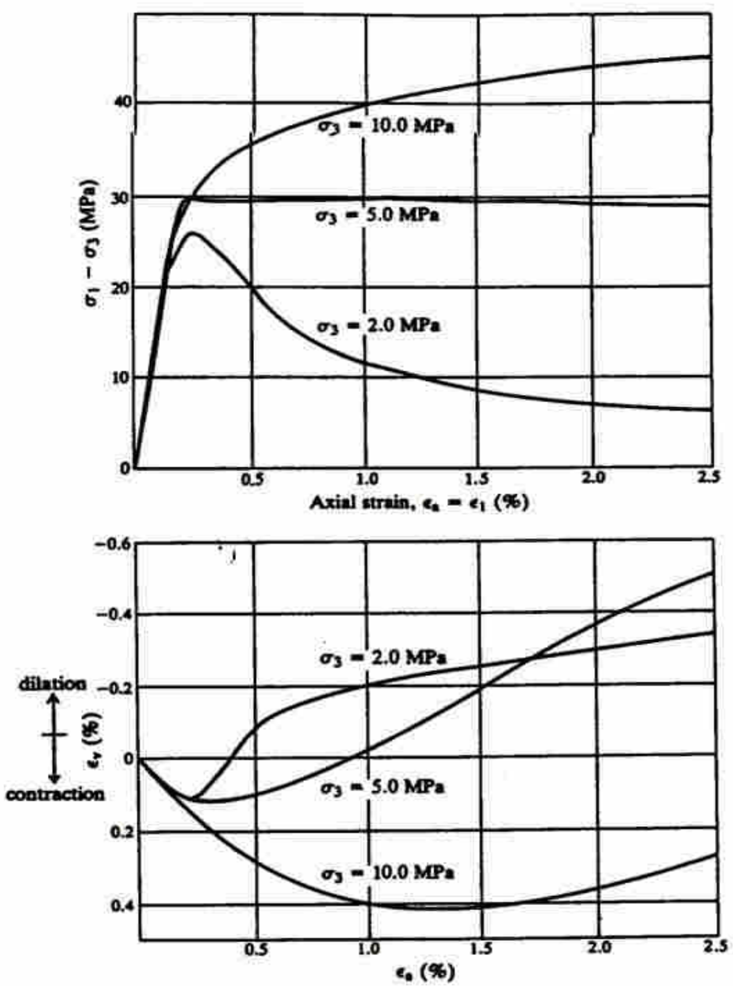

Figure 4.18 Results of triaxial compression tests on an oolitic limestone with volumetric strain measurement (after Elliott, 1982).

Shortly after the peak strength is reached, the net volumetric strain of the specimen becomes dilational. Dilation continues in the post-peak range. The amount of dilation decreases with increasing confining pressure.

4.4.3 Triaxial compression ($\sigma_1 > \sigma_2 = \sigma_3$)

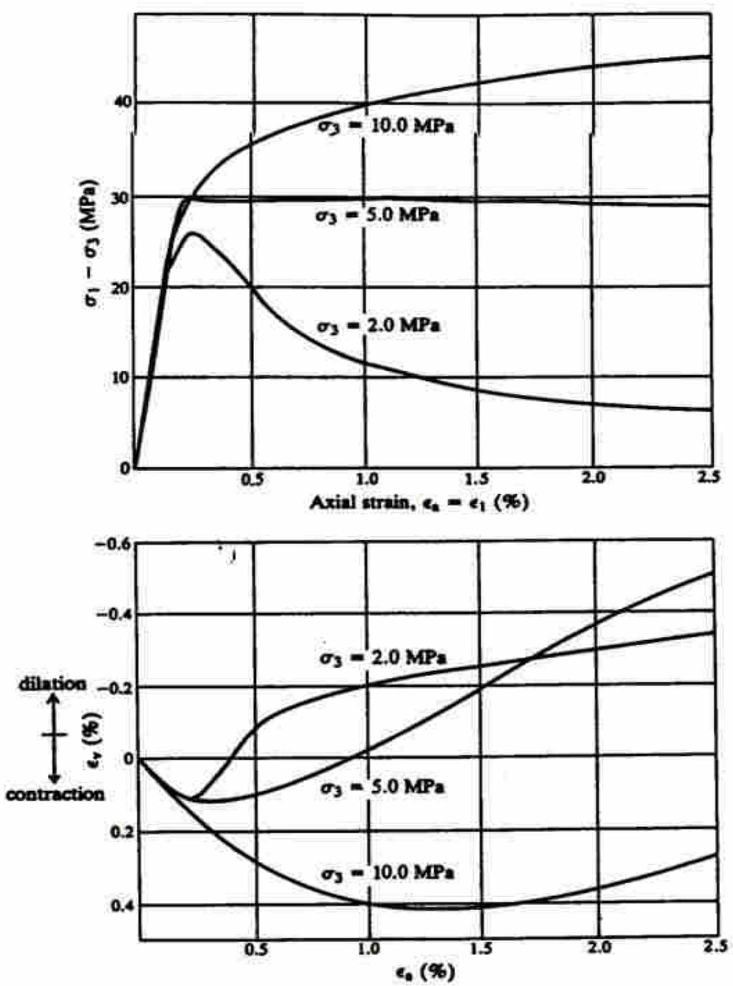

Figure 4.18 Results of triaxial compression tests on an oolitic limestone with volumetric strain measurement (after Elliott, 1982).

At very high confining pressures, often outside the range of engineering interest, dilation may be totally suppressed with the volumetric strains remaining contractile throughout the test.

4.4.3 Triaxial compression ($\sigma_1 > \sigma_2 = \sigma_3$)

Figure 4.19 illustrates a number of other important features of the behaviour of rock in triaxial compression.

Figure 4.19 Complete axial stress–axial strain curves obtained in triaxial compression tests on Tennessee Marble at the confining pressures indicated by the numbers on the curves (after Wawersik and Fairhurst, 1970).

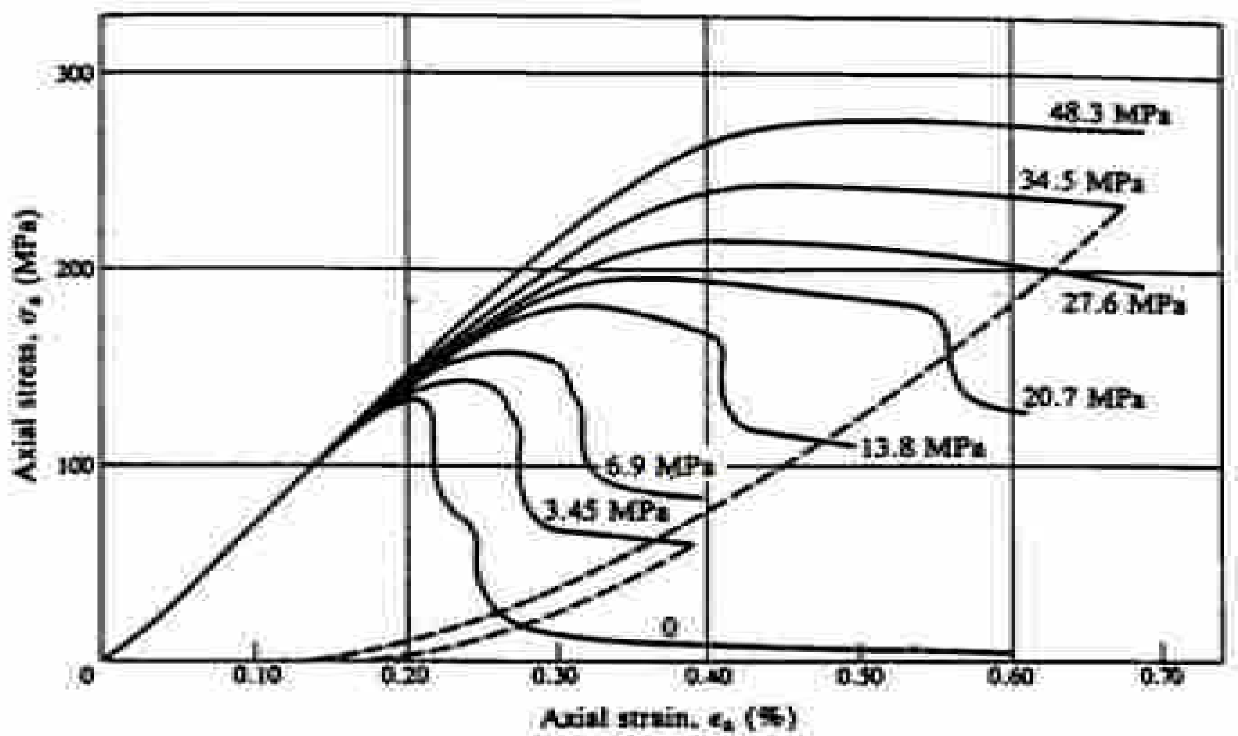

4.4.3 Triaxial compression ($\sigma_1 > \sigma_2 = \sigma_3$)

These and similar data for other rocks show that,

with increasing confining pressure,

- (a) the peak strength increases;
- (b) there is a transition from typically brittle to fully ductile behaviour with the introduction of plastic mechanisms of deformation including cataclastic flow and grain-sliding effects;

Figure 4.19 Complete axial stress -axial strain curves obtained in triaxial compression tests on Tennessee Marble at the confining pressures indicated by the numbers on the curves (after Wawersik and Fairhurst, 1970).

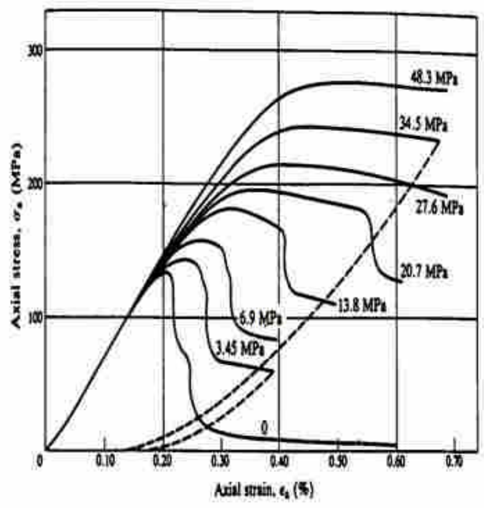

4.4.3 Triaxial compression ($\sigma_1 > \sigma_2 = \sigma_3$)

These and similar data for other rocks show that, with increasing confining pressure,

(c) the region incorporating the peak of the (σ_a - ε_a) curve flattens and widens;

(d) the post-peak drop in stress to the residual strength reduces and disappears at high values of σ_3 .

Figure 4.19 Complete axial stress -axial strain curves obtained in triaxial compression tests on Tennessee Marble at the confining pressures indicated by the numbers on the curves (after Wawersik and Fairhurst, 1970).

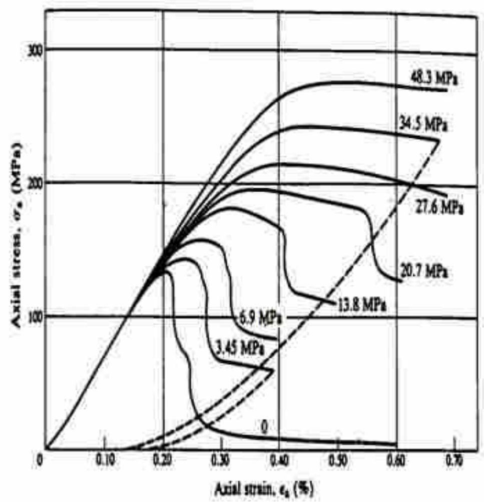

4.4.3 Triaxial compression ($\sigma_1 > \sigma_2 = \sigma_3$)

The confining pressure at which the post-peak reduction in strength disappears and the behaviour becomes fully ductile (σ_3 = 48.3 MPa in Figure 4.19), is known as the brittle-ductile transition pressure and varies with rock type.

4.4.3 Triaxial compression ($\sigma_1 > \sigma_2 = \sigma_3$)

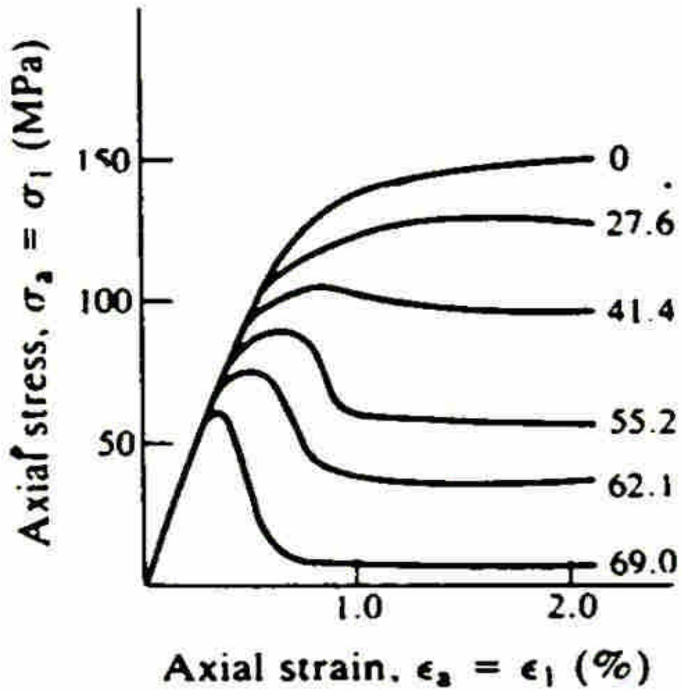

Figure 4.20 Effect of pore pressure (given in MPa by the numbers on the curves) on the stress–strain behaviour of a limestone tested at a constant confining pressure of 69 MPa (after Robinson, 1959).

The influence of pore-water pressure

4.4.3 Triaxial compression ($\sigma_1 > \sigma_2 = \sigma_3$)

Brace and Martin (1968) conducted triaxial compression tests on a variety of crystalline silicate rocks of low porosity (0.001- 0.03) at axial strain rates of $10^{-3} - 10^{-8}\ s^{-1}$. They found that the classical effective stress law held only when the strain rate was less than some critical value which depended on the permeability of the rock, the viscosity of the pore fluid and the specimen geometry. At strain rates higher than the critical, static equilibrium could not be achieved throughout the specimen.

4.4.4 Polyaxial compression ($\sigma_1 > \sigma_2 > \sigma_3$)

These tests may be carried out on cubes or rectangular prisms of rock with different normal stresses being applied to each pair of opposite faces. The results of polyaxiai compression tests on prismatic specimens are often conflicting, but generally indicate some influence of the intermediate principal stress, σ_2 , on stress-strain behaviour.

4.4.4 Polyaxial compression ($\sigma_1 > \sigma_2 > \sigma_3$)

Generally, the peak strength increases with increasing σ_2 for constant σ_3, but the effect is not as great as that caused by increasing σ_3 by a similar amount (Paterson, 1978). However, doubts must remain about the uniformity of the applied stresses in these tests and the results should be interpreted with great care.

4.4.5 Influence of stress path

A test of considerable relevance in this regard is the triaxial extension test which is carried out in a triaxial cell with the confining pressure, σ_r ,greater than the axial stress, σ_a . The test may be commenced at $\sigma_a = \sigma_r$ with σ_a , being progressively reduced so that $\sigma_r = \sigma_1 = \sigma_2 > \sigma_a = \sigma_3$. With modern servo-controlled testing machines, almost any desired total or effective stress path can be followed within the limitations imposed by the axisymmetric configuration of the triaxial cell.

4.4.5 Influence of stress path

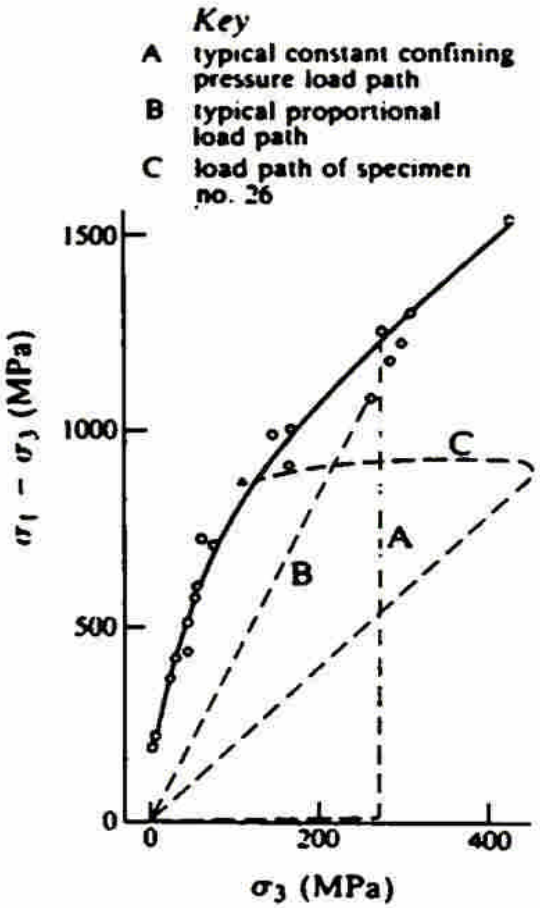

Figure 4.21 Influence of stress path on the peak strength envelope for Westerly Granite (after Swanson and Brown, 1971).

- Swanson and Brown (1971) investigated the effect of stress path on the peak strength of a granite and a quartz diorite. They found that, for both rock types, the peak strengths in all tests fell on the same envelope (Figure 4.21 for Westerly Granite) irrespective of stress path. They also found that the onset of dilatancy, described in section 4.4.3, is stress-path independent. Similarly, Elliott (1982) found the yield locus of a high-porosity, oolitic limestone to be stress-path independent.

4.5 Strength criteria for isotropic rock material
4.5.1 Types of strength criterion

Peak Strength Criterion ：A relation between stress components which will permit the peak strengths developed under various stress combinations to be predicted.

Residual Strength Criterion ： be used to predict residual strengths under varying stress conditions.

Yield Criterion ：A relation between stress components which is satisfied at the onset of permanent deformation.

Strength and yield criteria are best written in effective stress **form**

4.5 Strength criteria for isotropic rock material
4.5.1 Types of strength criterion

The general form of the peak strength criterion should be

$$\sigma_1 = f(\sigma_2, \sigma_3)$$

This is sometimes written in terms of the shear and normal stresses, a on a particular plane in the specimen

$$\tau = f(\sigma_n)$$

All of the criteria used in practice are reduced to the form

$$\sigma_1 = f(\sigma_3)$$

4.5.2 Coulomb's shear strength criterion

$$s = c + \sigma_n \tan \phi \qquad \textbf{(4.11)}$$

where c = cohesion and ϕ =angle of internal friction.

$$\sigma_n = \frac{1}{2}(\sigma_1 + \sigma_3) + \frac{1}{2}(\sigma_1 - \sigma_3)\cos 2\beta$$

and

$$\tau = \frac{1}{2}(\sigma_1 - \sigma_3)\sin 2\beta$$

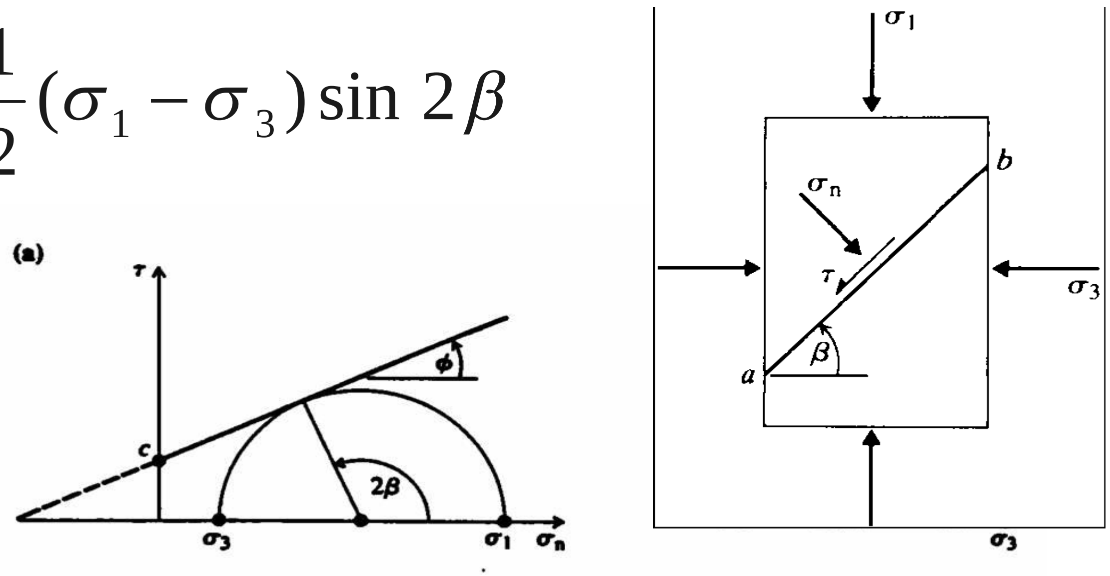

Figure 4.23 Coulomb strength envelopes in terms of (a) shear and normal stresses, and (b) principal stresses.

4.5.2 Coulomb's shear strength criterion

Substitution for σ_n and $s = \tau$ in equation 4.11 and rearranging gives the limiting stress condition on any plane defined by β as

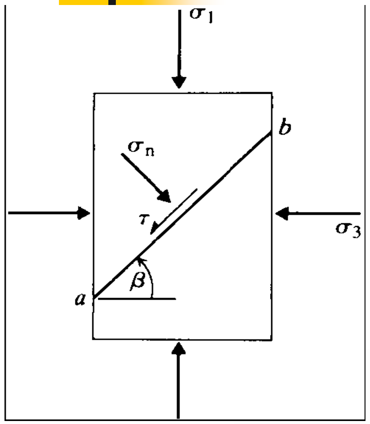

$$\sigma_1 = \frac{2c + \sigma_3 \left[\sin 2\beta + \tan\phi \left(1 - \cos 2\beta \right) \right]}{\sin 2\beta - \tan\phi \left(1 + \cos 2\beta \right)} \qquad (4.12)$$

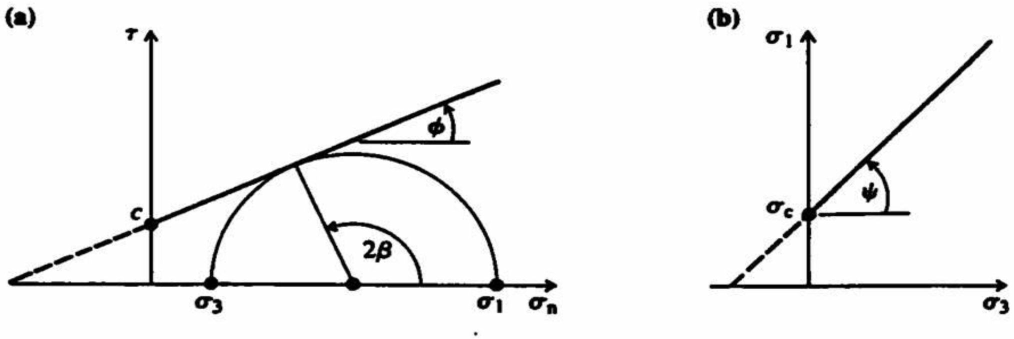

Figure 4.23 Coulomb strength envelopes in terms of (a) shear and normal stresses, and (b) principal stresses.

$$\sigma_1 = \frac{2c + \sigma_3\left[\sin 2\beta + \tan\phi\left(1 - \cos 2\beta\right)\right]}{\sin 2\beta - \tan\phi\left(1 + \cos 2\beta\right)}$$

4.5.2 Coulomb's shear strength criterion

The Mohr circle construction of Figure 4.23a gives the orientation of this critical plane as

$$\beta = \frac{\pi}{4} + \frac{\phi}{2}$$

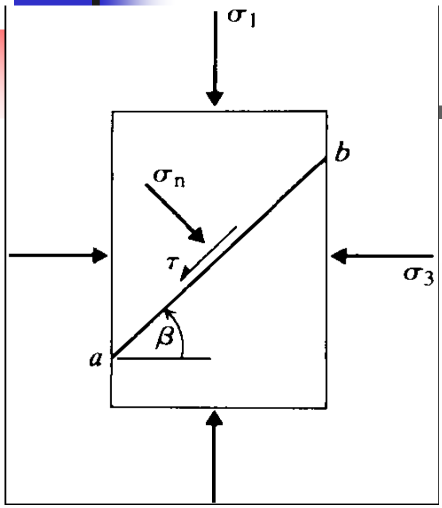

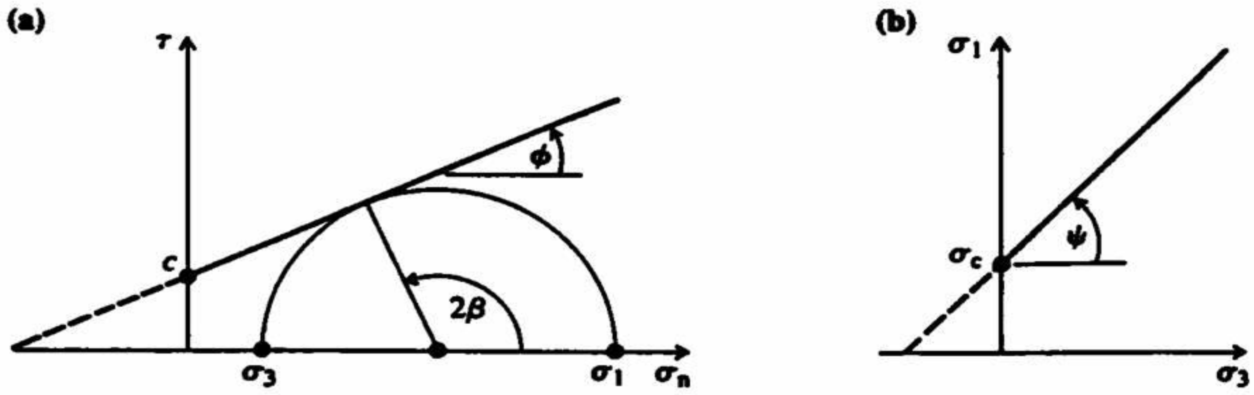

Figure 4.23 Coulomb strength envelopes in terms of (a) shear and normal stresses, and (b) principal stresses.

$$\sigma_1 = \frac{2c + \sigma_3\left[\sin 2\beta + \tan\phi\left(1 - \cos 2\beta\right)\right]}{\sin 2\beta - \tan\phi\left(1 + \cos 2\beta\right)}$$

4.5.2 Coulomb's shear strength criterion

$$\beta = \frac{\pi}{4} + \frac{\phi}{2}$$

For the critical plane, $\sin 2\beta = \cos\phi$, $\cos 2\beta = -\sin\phi$

, and equation 4.12 reduces to

$$\sigma_1 = \frac{2c\cos\phi + \sigma_3(1 + \sin\phi)}{1 - \sin\phi} \qquad \textbf{(4.14)}$$

$$\sigma_1 = \sigma_3 K_p + 2c\sqrt{K_p}$$

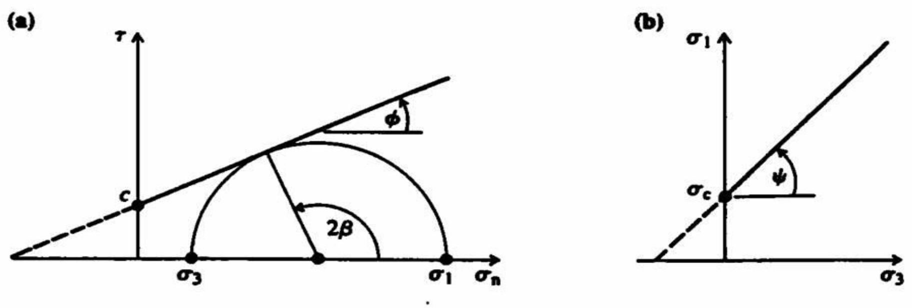

Figure 4.23 Coulomb strength envelopes in terms of (a) shear and normal stresses, and (b) principal stresses.

4.5.2 Coulomb's shear strength criterion

The **Slope** of （b） linera equation of σ_1 σ_3

$$\tan\psi = \frac{1+\sin\phi}{1-\sin\phi} = K_p$$

interception (4.15)

$$\sigma_c = \frac{2c\cos\phi}{1-\sin\phi} = 2c\sqrt{K_p}$$

(4.16)

Figure 4.23 Coulomb strength envelopes in terms of (a) shear and normal stresses, and (b) principal stresses.

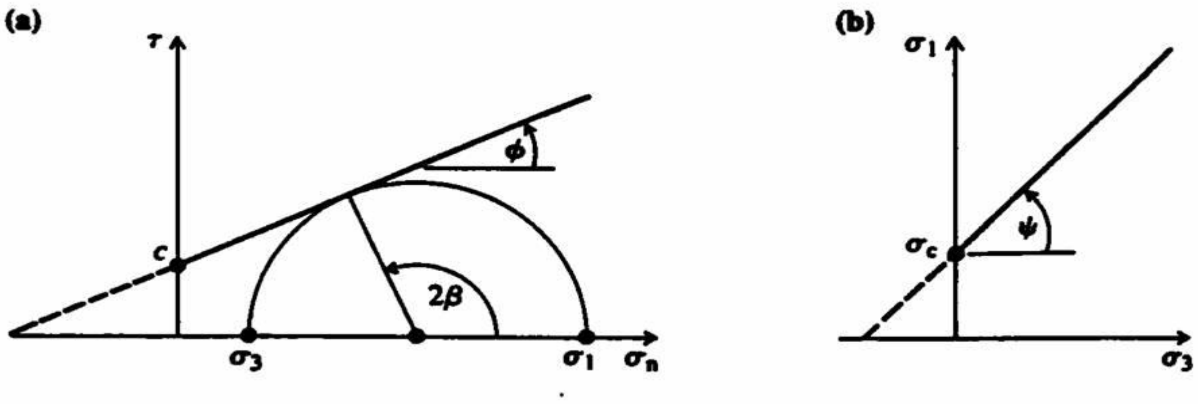

4.5.2 Coulomb's shear strength criterion

If the Coulomb envelope shown in Figure 4.23b is extrapolated to $\sigma_1 = 0$, it will intersect the σ_3 axis at an apparent value of uniaxial tensile strength of the material given by

$$\sigma_T = \frac{2c\cos\phi}{1+\sin\phi} \qquad \textbf{(4.17)}$$

Figure 4.23 Coulomb strength envelopes in terms of (a) shear and normal stresses, and (b) principal stresses.

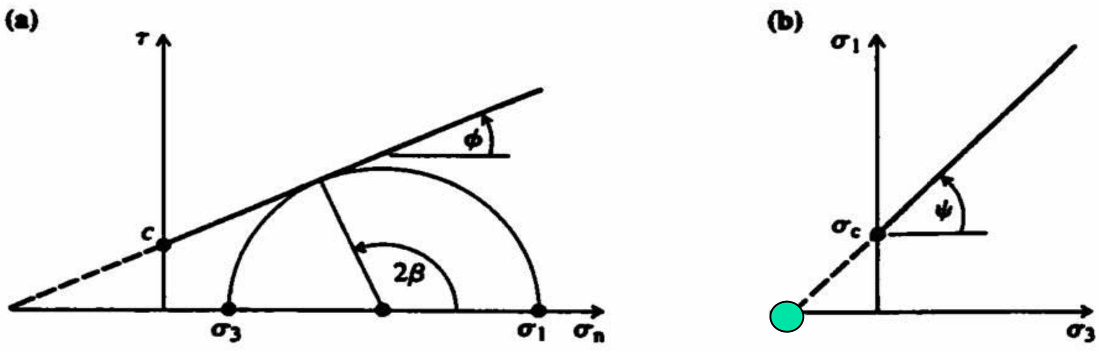

4.5.2 Coulomb's shear strength criterion

A tensile cutoff is usually applied at a selected value of uniaxiai tensile stress , as shown in Figure 4.24. For practical purposes, it is prudent to put $T_0 = 0$.

$$T_0 = 0$$

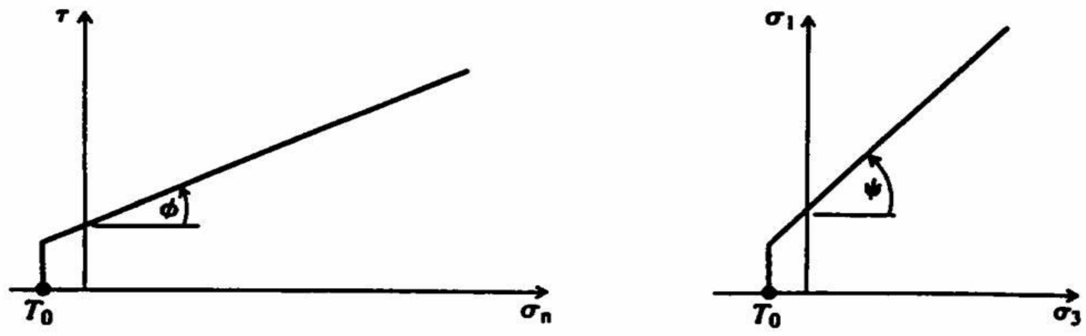

Figure 4.24 Coulomb strength envelopes with a tensile cut-off.

4.5.2 Coulomb's shear strength criterion

Although it is widely used, Coulomb's criterion is not a particularly satisfactory peak strength criterion for rock material. The reasons for this are:

(a) It implies that a major shear fracture exists at peak strength. Observations such as those made by Wawersik and Fairhurst (1970) show that this is not always the case.

(b) It implies a direction of shear failure which does not always agree with experimental observations.

(c) Experimental peak strength envelopes are generally non-linear. They can be considered linear only over limited ranges of σ_n or σ_3 .

4.5.2 Coulomb's shear strength criterion

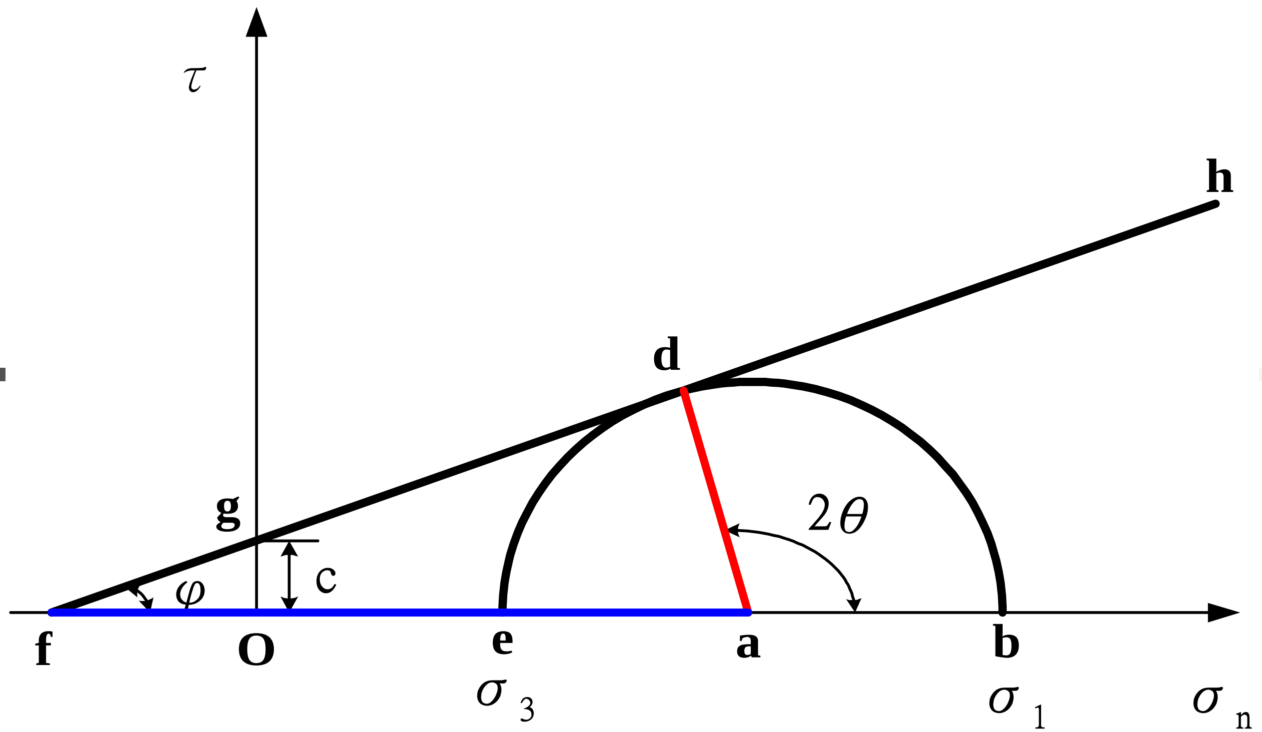

$$\angle bad = 2\theta = 90 + \phi$$

$$\theta = 45 + \frac{\phi}{2}$$

4.5.2 Coulomb's shear strength criterion

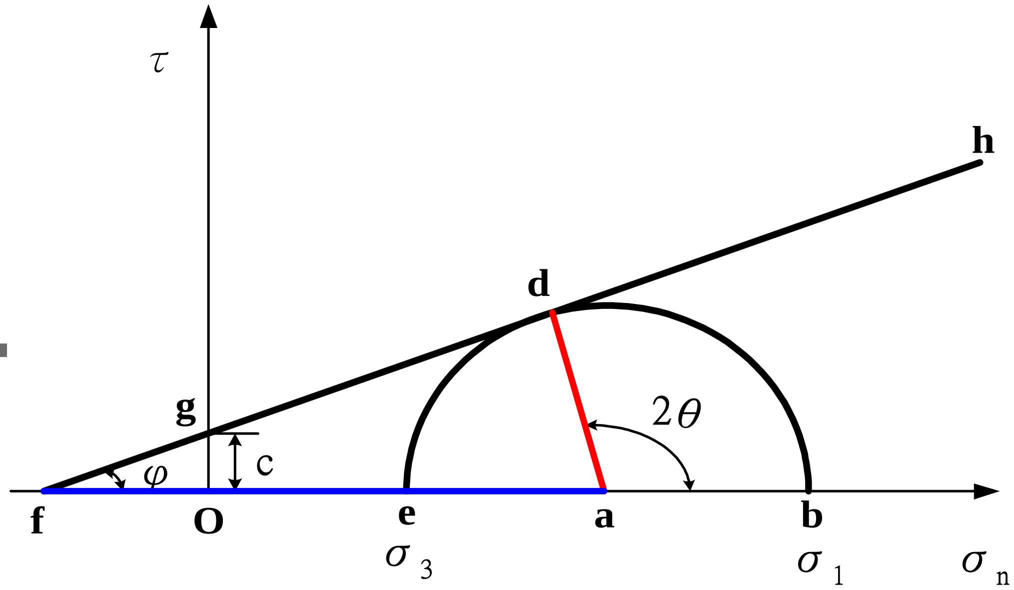

$$\frac{\overline{ad}}{\overline{fa}} = \sin\phi$$

$$\overline{fa} = \overline{fO} + \overline{Oa} = c\cot\phi + \frac{\sigma_1 + \sigma_3}{2}$$

4.5.2 Coulomb's shear strength criterion

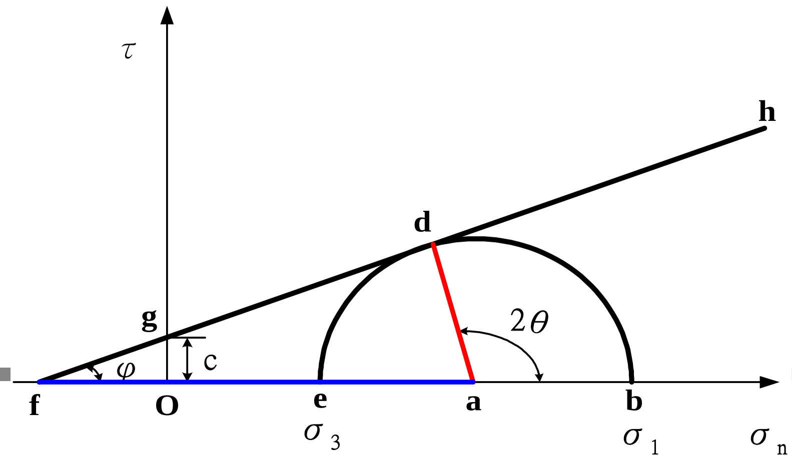

$$\overline{ad} = \frac{\sigma_1 - \sigma_3}{2} \quad (5)$$

Substituting for Eq.(4) and Eq.(5) in Eq.(3) gives

$$\sin\phi = \frac{\frac{\sigma_1 - \sigma_3}{2}}{c\cot\phi + \frac{\sigma_1 + \sigma_3}{2}} \quad (6)$$

4.5.2 Coulomb's shear strength criterion

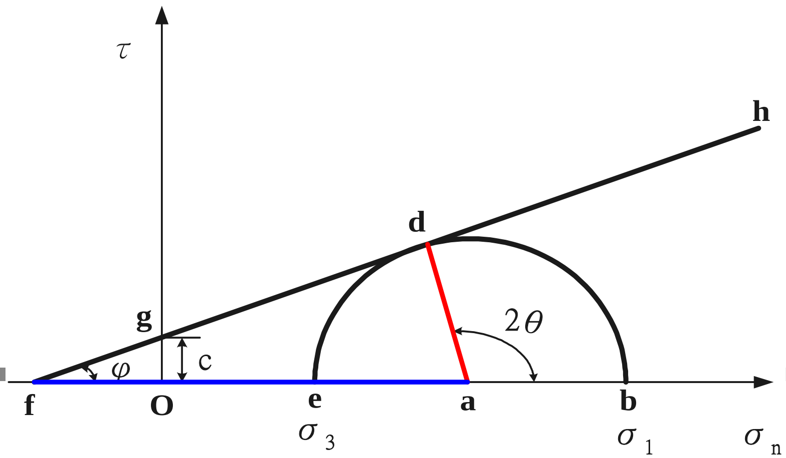

Eq.(6) reduces to

$$\sigma_1 = \sigma_3\left(\frac{1+\sin\phi}{1-\sin\phi}\right) + 2c\sqrt{\left(\frac{1+\sin\phi}{1-\sin\phi}\right)} \qquad \textbf{(7)}$$

or

$$\sigma_1 = \sigma_3 \tan^2(45+\frac{\phi}{2}) + 2c\tan(45+\frac{\phi}{2}) \qquad \textbf{(8)}$$

or

$$\sigma_1 = \sigma_3 K_p + 2c\sqrt{K_p} \qquad \textbf{(9)}$$

4.5.2 Coulomb's shear strength criterion

某一岩層，強度受莫耳－庫倫((**Mohr－Coulomb**)破壞準則控制，其凝聚力**C=20MPa**，內摩擦角ϕ**=40º**，今受到最大主應力爲**100Mpa**，最小主應力爲**15MPa**的應力作用。

(一)試證明該一岩層在此應力狀況下是穩定的。

$$\sigma_1 = \sigma_3\left(\frac{1+\sin\phi}{1-\sin\phi}\right) + 2c\sqrt{\left(\frac{1+\sin\phi}{1-\sin\phi}\right)} = \sigma_3 K_p + 2c\sqrt{K_p}$$

$$= 15 \times 4.6 + 2 \times 20 \times \sqrt{4.6}$$

$$= 154.8\,MPa \;>\; 100\,MPa$$

故穩定

4.5.2 Coulomb's shear strength criterion

某一岩層，強度受莫耳－庫倫((**Mohr－Coulomb**)破壞準則控制，其凝聚力**C=20MPa**，內摩擦角ϕ**=40º**，今受到最大主應力為**100Mpa**，最小主應力為**15MPa**的應力作用。

(二)假設孔隙水壓由零開始上升，直到破壞發生，試問破壞時之孔隙水壓力大小為何？

$$(\sigma_1 - U_f) = (\sigma_3 - U_f)K_p + 2c\sqrt{K_p}$$

$$(100 - U_f) = (15 - U_f)4.6 + 2 \times 20 \times \sqrt{4.6}$$

$$3.6 \times U_f = 54.78$$

$$U_f = 15.22\,MPa$$

4.5.2 Coulomb's shear strength criterion

某一岩層，強度受莫耳－庫倫((**Mohr－Coulomb**)破壞準則控制，其凝聚力**C=20MPa**，內摩擦角ϕ **=40º**，今受到最大主應力爲**100Mpa**，最小主應力爲**15MPa**的應力作用。

(三)破壞時，斷裂面上的有效正應力與剪應力分別是多少？

$$\alpha = 45 + \frac{\phi}{2} = 65$$

$$\sigma_n = \frac{\sigma_1 + \sigma_3}{2} - \frac{\sigma_1 - \sigma_3}{2}\cos(\pi - 2 \times 65) = 15\,MPa$$

$$\tau = \frac{\sigma_1 - \sigma_3}{2}\sin(\pi - 2 \times 65) = 32.56\,MPa$$